THE INFLUENCE OF FRACTURE MODE TRANSITION ON THE COMPLIANCE OF THIN SECTION FRACTURE SPECIMENS

D. Rhodes, L. E. Culver and J. C. Radon

Department of Mechanical Engineering, Imperial College of Science & Technology, Exhibition Road, London SW7 2BX, UK

ABSTRACT

Cyclic and monotonic crack propagation tests have been carried out on 6 mm and 9.5 mm thick compact tension specimens of BS.L97 (2024-T3) and DTD.5120 (7010-T7651) aluminium alloys. Crack lengths were measured optically, and also from the specimen compliance, and the results compared. It is shown that the difference between these measurements is generally less than the theoretical plane stress plastic zone size and may not exceed the specimen thickness unless a 45° slant crack is formed. Some suggestions are made with regard to "plastic zone corrections" in fracture analysis of thin sheet structures, and the estimation of K_c values.

KEYWORDS

Fracture; plane stress; aluminium alloys; fatigue; fracture mode.

INTRODUCTION

Crack propagation tests under both cyclic and monotonic loading have been carried out on thin section aluminium alloy specimens under predominantly linear elastic conditions. At high stress intensity factors, the mechanisms of both fatigue and stable crack growth are dominated by ductile tearing (micro-void coalescence) within a small process zone. It may be supposed, then, that fatigue cracking and 'R-curve' data would be identical in this region if they were both represented by the same parameters. Conventionally, of course, fatigue crack growth data are represented as log (da/dN) versus log (ΔK), and R-curves as K_R versus $\Delta a'$. The two may, however, be plotted on the same axes. The relationship is complicated by two factors, the second of which will be dealt with in detail.

Reversed loading introduces a residual stress distribution close to the tip of a fatigue crack, which differs from that expected with a monotonically increasing loading at the same stress intensity factor. This effect has been studied in detail elsewhere and allows reasonable correlation to be obtained between R-curves and fatigue data at zero (Schwalbe, 1979) or non-zero (Rhodes, Radon & Culver, 1980a) stress ratios (Fig. 1).

In thin sections, a further complication arises, with the effects of fracture mode transition on the R-curve. Under these circumstances, the crack may be re-orientated to change from a square (mode I) to a slant (mixed mode I/III) fracture. If the plastic zone at the crack tip is embedded in a comparatively large, elastically deformed specimen, then the energy available for crack tip deformation, and hence crack propagation, is adequately represented by the linear elastic strain energy release rate, G. This may be derived from the specimen compliance and is independent of the orientation and shape of the crack tip. If the specimen compliance is C_s, then

$$G = \frac{P^2}{2B}\left(\frac{dC_s}{da}\right) \tag{1}$$

For plane stress conditions, the stress intensity factor is given by

$$K^2 = E\,G \tag{2}$$

so that a relationship may be expected, between crack extension and stress intensity factor, regardless of mode transition, provided that it is always derived from specimen compliance and not from the physical crack length.

If the specimen cannot be made sufficiently large to meet the requirement of a fully embedded plastic zone, the elastic parameter, G, must be replaced by some elasto-plastic variable, such as the J-integral. In the present study, specimen sizes have been chosen so that no significant difference would be expected. This is discussed in detail in the description of the test method.

THEORY

For monotonic loading, it will be shown that the increase in compliance measured crack length, $\Delta a'$, is indeed related to the crack growth resistance by, say

$$\Delta a' = F(K_R) \tag{3}$$

regardless of mode transition, strain rate, etc.

K_R may be evaluated in stress intensity units from

$$K_R = L\,f(a_o + \Delta a + \phi) \tag{4}$$

in which L = loading parameter, proportional to load or stress, for example
a_o = crack length, prior to loading
Δa = increase in physical crack length

and

$$\phi = a' - (a_o + \Delta a) \tag{5}$$

where a' = instantaneous crack length determined from compliance measurement

Under cyclic loading, it becomes very difficult to define the increase in compliance measured crack length, da'/dN. This could be related to the change in compliance during the loading half-cycle, or to the total change in compliance for a complete cycle, which is likely to be much smaller. In interpreting the results, care is needed in distinguishing between the total plastic zone size, r_y, and the reversed plastic zone size, Δr_y.

However, the increase in physical crack length, da/dN, is unambiguous. At high stress intensities, where the crack extension is dominated by ductile tearing, crack advance occurs during the loading half-cycle. Thus, for a stress ratio of zero, one may assume an equation corresponding to equation (3), e.g.

$$\frac{da}{dN} = F_f(K_{Rf}) \tag{6}$$

where K_{Rf} is the maximum crack growth resistance during the cycle, given by

$$K_{Rf} = L_{max}\, f(a + da/dN + \phi) \tag{7}$$

In order to match the fatigue crack growth curve to the R-curve, it is necessary to determine the relationship between F_f and F. Firstly, the difference between physical and compliance measured crack lengths must be taken into account. Secondly, allowance must be made for the residual stress distribution due to prior cycling which reduces the cyclic plastic zone size, but does not change the specimen compliance at maximum load. This term was evaluated in detail by Schwalbe (1979) and depends on the work hardening exponent, n, measured after plastic cycling to 'saturation'. Thus

$$F_f(K_{Rf}) = \left(\frac{2^{n+1}}{4}\right) [F(K_{Rf}) - \phi] \tag{8}$$

It will be seen that equations (4), (7) and (8) all include the term ϕ. Evaluation of this parameter is particularly important in thin section material, as it may vary with crack orientation.

The simplest approximation to ϕ is given by Irwin's (1968) theoretical plastic zone radius, which, for plane stress conditions is

$$\phi \simeq r_y = \left(\frac{1}{2\pi}\right)\left(\frac{K_R}{\sigma_y}\right)^2 \tag{9}$$

or, for plane stress conditions, is

$$\phi \simeq r_y \simeq \left(\frac{1}{6\pi}\right)\left(\frac{K_R}{\sigma_y}\right)^2 \tag{10}$$

dependent on Poisson's ratio.

A series of test measurements shows, however, that these represent little more than upper and lower bounds for ϕ, and that significant deviations from these lines may occur. It is also important to use a value of σ_y which takes due account of any cyclic strain hardening, or softening, resulting from preceding fatigue cycles.

TEST METHOD

Compact tension specimens were machined from 50 mm thick plate of aluminium alloys DTD.5120 (7010-T7651) and BS.L97 (2024-T3). The specimens were each 9.5 mm or 6 mm thick with an L-T grain orientation. The compositions and mechanical properties of these materials are given in Tables 1 and 2.

TABLE 1 Nominal Composition of Aluminium Alloys

Element	Zn	Mg	Cu	Zr	Mn	Cr	Fe	Si
7010 (% wt)	6.20	2.50	1.70	0.14	<0.03	<0.05	<0.15	<0.10
2024 (% wt)	0.25	1.50	4.40	-	0.60	-	0.50	0.50

TABLE 2 Mechanical Properties of Aluminium Alloys

L-T Properties	DTD.5120 (7010-T7651*)	BS.L97 (2024-T3)
0.2% Proof Stress (MN/m^2)	484	310
Ultimate Tensile Stress (MN/m^2)	544	430
Elongation (%)	12.1	>8
Tensile Modulus, E (GN/m^2)	74.3	72.0
Approx. Work Hardening Exponent, n	0.11	0.11
Plane Strain Toughness, K_{Ic} ($MN/m^{3/2}$)	36	49

* Alcan-Booth proprietry thermo-mechanical treatment

The specimen size was selected to ensure the validity of linear elastic fracture mechanics. This could be determined in a variety of ways. Fedderson (1971) recommended that the nominal width, W, of the specimen should exceed 27 r_y. Sullivan & Freed (1971) used this technique successfully on a range of materials using centre-cracked tension specimens. Alternatively, a nominal 'net section stress' may be estimated, and the specimens sized to keep this below the yield stress (Srawley & Brown, 1965). The two methods give similar results for conventional specimens, and both were applied in this study. The range of specimens available (Fig. 2) are of a standard profile (ASTM, 1978), but with the loading holes modified to allow the use of a common set of shackles for all sizes. By the above criteria, no yielding was expected for DTD.5120 specimens to CTA/105 or BS.L97 specimens to CTA/150. Some CTA/90 specimens of DTD.5120 have also been used, although not with very long cracks, and no difficulties have been encountered.

Cyclic and monotonic loading tests were carried out in an Instron 50 kN tensile test machine at two different crosshead displacement rates, $\dot{\delta}$. At 0.004 mm/s, both a travelling microscope and a remote compliance measurement were used to determine the crack length. At 0.4 mm/s, remote compliance measurement alone was used during monotonic loading. The same rate, $\dot{\delta}$, gave a fatigue cycle frequency of between 0.1 Hz and 0.5 Hz, depending on the specimen and crack length. The crack length was measured periodically using a travelling microscope, ×40. Fatigue data were also available from tests using a 60 kN Dowty servo-hydraulic test machine at 10 Hz.

The remote compliance, C_1, is given by

$$C_1 = \frac{\delta}{P} \tag{11}$$

where δ is the crosshead displacement, and P the applied load.

C_1 includes the machine and instrumentation compliance, C_o, and the specimen compliance, C_s. At an early stage in each test, the compliance was measured at a low load and known crack length. C_s was determined from a standard calibration curve, and subtracted from C_1 to give a value of C_o for that particular combination of machine, specimen and instrumentation. As C_o is not affected by crack length, this constant could be used for the entire test. Some specimens were re-checked to confirm that C_o did not vary with a, and data were found to be close to Saxena & Hudak's (1979) wide range calibration curve (Fig. 3).

As the error in measuring C_1 remains constant, effectively the accuracy in determining a' tends to increase as the crack grows, and dC/da increases. This advantage is offset by the reduction in load capacity within the limits of the linear elastic assumptions as the crack becomes long. R-curve tests were started in general with $0.4 < a_o/W < 0.5$.

RESULTS

Conventional R-curve data are presented for both alloys in Fig. 4. It is interesting to note that the increase in $\dot{\delta}$, from 0.004 mm/s to 0.4 mm/s, caused the transition from square to slant fracture to take place over a shorter length of specimen, but only affected the curve of $\Delta a'$ versus K_R at points beyond nominal instability (i.e. beyond the maximum load condition). At the lower loading rate, mode transition did not occur at all in BS.L97 specimens, although it did in the fast tests. Where transition did not take place, there was an increased tendency for the crack to 'tunnel' with the crack tip advancing further at the core of the specimen than at the surface. Where this occurred, a nominal average crack length was used to evaluate the physical crack length, a, estimated from surface markings on the fractured specimen. This rate effect was demonstrated further by running a fatigue test to a high ΔK, so that transition occurred, and then carrying out a slow R-curve test. In such cases, a reversed 'slant-to-square' transition occurred at the outset of the R-curve test.

The slow monotonic loading data have been used to measure values of ϕ during stable crack growth. Figure 5 shows ϕ/B plotted against $1/B\,(K_R/\sigma_y)^2$. For equation (9), the data should fall on a line of slope $1/2\pi$ and for equation (10) on a slope of $1/6\pi$. In practice, the following trends were observed.

(i) The theoretical plane stress plastic zone size represents an upper limit for values of ϕ.

(ii) The value of ϕ cannot exceed the specimen thickness, B, unless transition to a fully developed 45° plane is complete.

(iii) During monotonic loading, the value of ϕ may remain constant, equal to the specimen thickness, while mode transition occurs, but the transition may commence long before the condition is reached.

The results of a slow cyclic test are shown in Fig. 6. The material was BS.L97 and no mode transition occurred. The machine was controlled manually with the load reduced to one tenth of its maximum value in each 'trough' and then increased to give the same crack extension in the next cycle. In each case, the maximum

load condition was passed. There was no significant change in the $\Delta a'$ versus K_R curve, compared with Fig. 4, but the Δa versus K_R curve (Fig. 6) does show a reduction in crack extension after cycling.

DISCUSSION

In order to extend the data to very large values of ϕ/B, etc., it is necessary to consider thinner sections, for which a fully developed slant fracture is expected throughout the tests. Tests on 1.6 mm thick BS.L109 (2024-T3 Al clad sheet) are now in progress, using compact tension specimens held between lubricated steel plates to prevent buckling. The expected trend of results for monotonic loading cases is indicated by published data from other sources.

Bradshaw & Wheeler (1974) and Wheeler, Wood & Bradshaw (1974) used centre cracked tension (CCT) specimens, and also compact tension specimens, with the ratio $2H/W = 1.9$ (c.f. Fig. 2). This is said to give better crack path stability than the ASTM standard, which has $2H/W = 1.2$. The CT2/30, CT2/120 and CT2/240 specimens have W = 30 mm, 120 mm and 240 mm, respectively. Heyer & McCabe (1972) used standard crack line wedge loaded (CLWL) specimens. Their results are indicated in Fig. 7. Moving from the large CCT specimens, through progressively smaller CT specimens to the CLWL tests, the loading and buckling constraints become more severe and the value of ϕ decreases. Even in the CCT case, it is only about two thirds of the theoretical plane stress value.

These results may now be considered in comparison with results from the present study (Fig. 5). For plane strain conditions, ASTM standards (1974) require that the thickness, $B < 2.5\ (K/\sigma_y)^2$, which is indicated in Fig. 5. Most points lying just above this condition have values of ϕ close to the theoretical plane stress line. As the crack extends and mode transition commences, the slope gradually decreases as described above.

The dependence of transition characteristics on loading rate and loading constraint is not entirely clear, but there are some consistent trends. Mode transition normally occurs by the progressive development of shear lips, which eventually meet so that they cover the entire specimen. During fatigue cracking, the transition more usually occurs by gradual 'rotation' of the crack from a square to a 45° slant plane. In every case, an increase in loading rate causes a reduction in the amount of crack growth required to complete the transition. A comparison of fatigue crack surfaces with those obtained at 10 Hz confirms this trend. Despite this, mode transition always began at a crack growth rate of about 9×10^{-4} mm/cycle in 9.5 mm DTD.5120 and 5.5×10^{-4} mm/cycle in 9.5 mm BS.L97, regardless of stress ratio or frequency. This result agrees with early work by Broek & Schijve (1963).

The low speed cyclic tests demonstrate the trend to reduce the physical crack extension during loading in consecutive cycles. The dashed line of Fig. 6 shows that Schwalbe's (1979) factor of $2^{n+1}/4$ is a good estimate. As there was no change in the compliance measured crack length due to prior cycling (i.e. ϕ has increased), there was no change in the load required for instability. If the critical engineering stress intensity factor is defined as

$$K_{eng_c} = L_{max}\, f(a_o) \tag{12}$$

it may be shown that (Rhodes, Radon & Culver, 1980a, 1980b)

$$K_{eng_c} \simeq \left[\frac{1}{m\,C}\,\frac{f(a_o)}{f'(a_o)}\right]^{1/m} \tag{13}$$

where the R-curve is approximated by

$$\Delta a = C\,K_R^{\,m} \tag{14}$$

Figure 8 shows K_{eng_c} plotted against $f(a_o)/f'(a_o)$ for a variety of 2024-T3 alloys specimens. The K_{eng_c} data include CCT, standard and non-standard CT specimens (some taken from Bradshaw & Wheeler (1974)), and those marked with square symbols are for the second, third and fourth cycles shown in Fig. 6. It will be seen that they fall within the general scatter of data.

APPLICATIONS

Current practice in fracture analysis of large thin sheet structures (ESDU, 1976) is based on linear elastic fracture mechanics, with a 'plastic zone correction'. Typically, for monotonic loading one would use

$$K = L\,f(a + r_y) \tag{15}$$

In cyclic loading cases, the reversed plastic zone size replaces r_y with

$$\Delta r_y = \frac{2^{n+1}}{4}\left(\frac{\Delta K}{\sigma_y}\right)^2 \tag{16}$$

usually taking $n = 0$, i.e. neglecting work hardening.

The present work suggests that equation (13) is justified for $\phi < B$, but is often over-conservative for $\phi > B$. Under cyclic loading, it is suggested that ϕ should be calculated in the same way, but substituting the maximum value of K and the cyclically saturated value of σ_y, σ_{yf}, e.g.

$$\phi = \frac{1}{2\pi}\left[\frac{\Delta K}{(1-R)\,\sigma_{yf}}\right]^2 \qquad \text{for } \phi < B \tag{17}$$

CONCLUSIONS

For the materials and thicknesses tested, it was concluded that

(a) The difference, ϕ, between the physical and compliance measured crack lengths never exceeds the theoretical plastic zone size.

(b) ϕ may only exceed the specimen thickness if the crack is on a 45° (slant) plane.

(c) Square-to-slant transition may begin while ϕ is less than the thickness.

(d) Crack extension in fatigue at high stress intensities is related to the

reversed plastic zone size.

ACKNOWLEDGEMENTS

The authors wish to acknowledge financial assistance from British Aerospace (Aircraft Group) and the Science Research Council.

REFERENCES

ASTM (1974). Test method for plane strain fracture toughness of metallic materials. *Standard E399-74*, American Society for Testing and Materials.

ASTM (1978). Tentative test method for constant-load-amplitude fatigue crack growth rates above 10^{-8} m/cycle. *Standard E647-78T*, American Society for Testing and Materials.

Bradshaw, F.J., and C. Wheeler (1974). The crack resistance of some aluminium alloys, and the prediction of thin section failure. *Tech. Report 73191*, Royal Aircraft Establishment, Farnborough.

Broek, D., and J. Schijve (1963). The influence of the mean stress on the propagation of fatigue cracks in aluminium alloy sheet. *Report No. NLR-TR-M2111*, National Aerospace Laboratory, NLR, Amsterdam.

ESDU (1976). Estimation of fatigue crack growth rate, and residual strength of components, using linear elastic fracture mechanics. *Data Item 76019*, Engineering Sciences Data Unit, London.

Fedderson, C. (1971). Some developments in residual strength analysis. *ASTM STP486*.

Heyer, R.H., and D.E. McCabe (1972). Plane stress fracture toughness testing, using a crack line loaded specimen. *Eng. Fract. Mech.*, 4, 393-412.

Irwin, G.R. (1968). Linear fracture mechanics, fracture toughness and fracture control. *Eng. Fract. Mech.*, 1, 241-257.

Rhodes, D., J.C. Radon, and L.E. Culver (1980a). Cyclic and monotonic crack propagation in a high toughness aluminium alloy. *Int. J. Fatigue*, 2,

Rhodes, D., J.C. Radon, and L.E. Culver (1980b). On the geometry dependence of fracture toughness, K_c. In preparation.

Saxena, A., and S.J. Hudak, Jr. (1978). Review and extension of compliance information for common crack growth specimens. *Int. J. Fracture*, 14, 453-467.

Schwalbe, K.-H. (1979). Some properties of stable crack growth. *Eng. Fract. Mech.*, 11, 331-342.

Srawley, J.E., and W.F. Brown (1965). Fracture toughness testing. *ASTM STP381*.

Sullivan, A.M., and C.N. Freed (1971). The influence of geometric variables on K_c values for two thin sheet aluminium alloys. *Report No. 7270*, Naval Research Laboratory, Washington, D.C.

Wheeler, C., R.A. Wood, and F.J. Bradshaw (1974). Some crack resistance curves of sheet compact tension specimens of aluminium alloys 7475-T761, 2024-T3 and 2024-T81. *Tech. Report 74086*, Royal Aircraft Establishment, Farnborough.

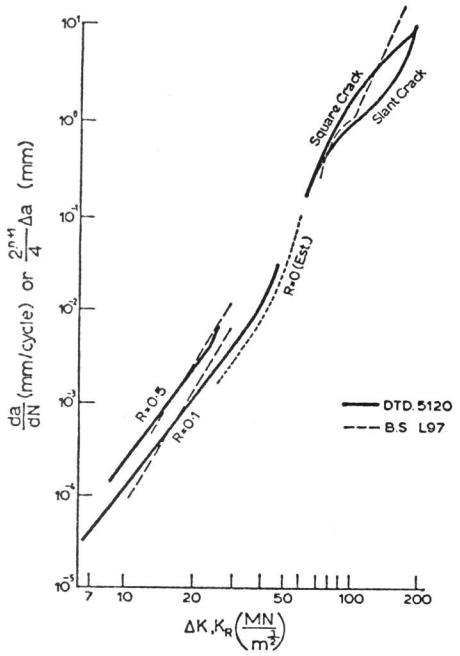

Fig. 1 Crack growth curves

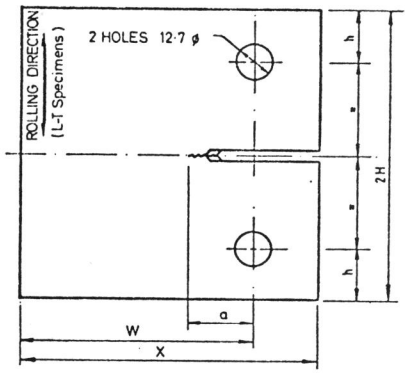

Dimensions in mm:

	W	X	2H	h
CTA/90	91	114	110	20
CTA/105	107	133	128	25
CTA/150	152	190	183	25

Fig. 2 CT test specimen

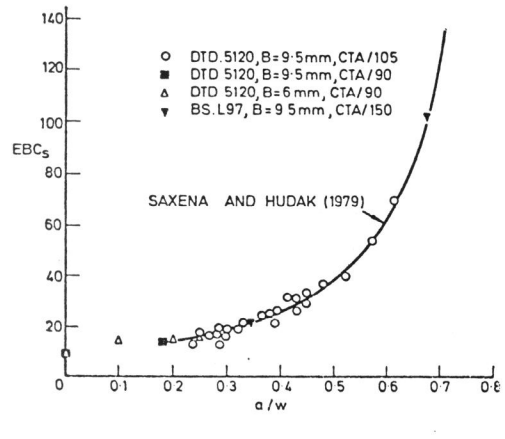

Fig. 3 Specimen compliance

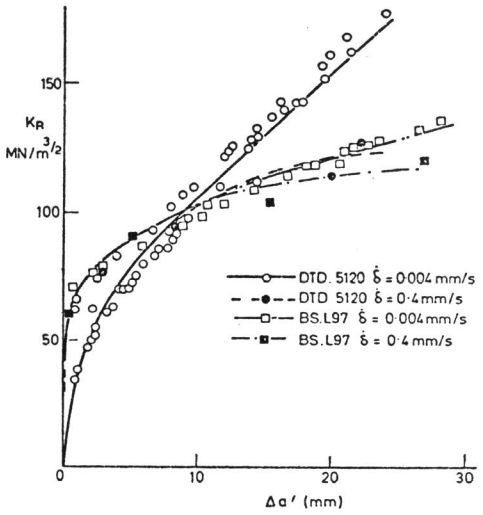

Fig. 4 Monotonic R-curve data

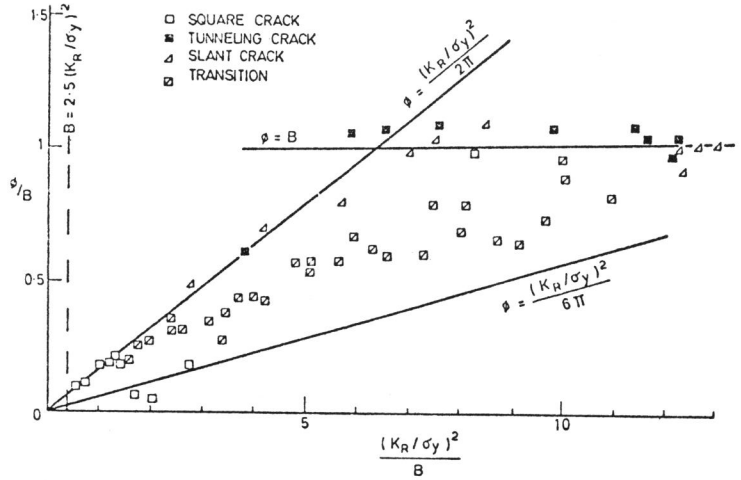

Fig. 5 Increase of ϕ with K_R

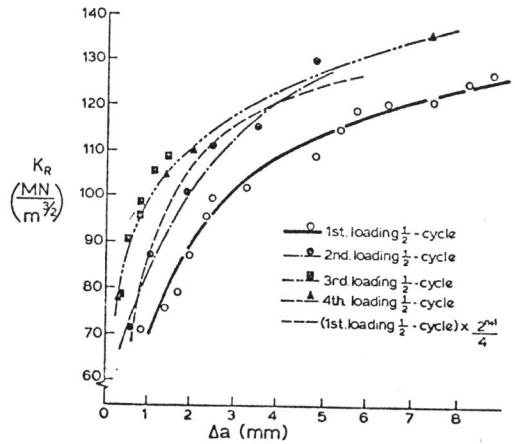

Fig. 6 R-curves for slow cyclic test (L97)

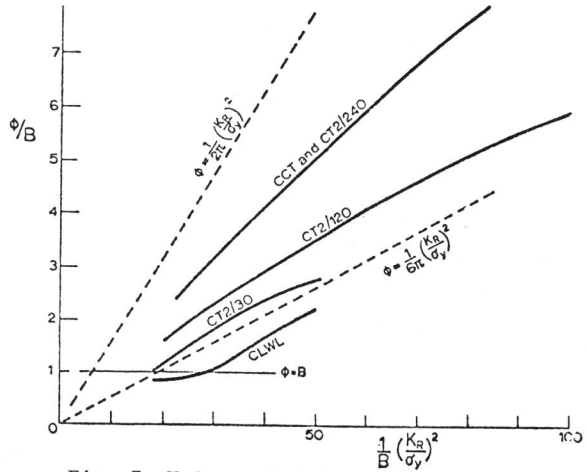

Fig. 7 Values of ϕ for thin sheet specimens (2024-T3)

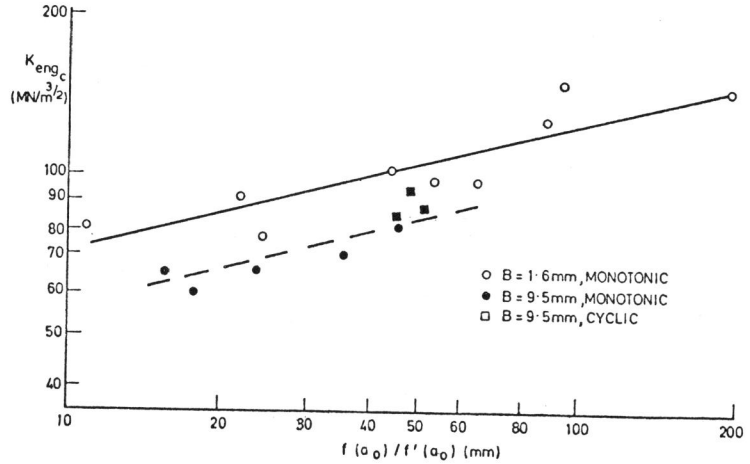

Fig. 8 Geometry dependence of K_c (2024-T3)